Research Square

Preprints are preliminary reports that have not undergone peer review.
They should not be considered conclusive, used to inform clinical practice,
or referenced by the media as validated information.

DJAMILAR: Geometric Charge and the Evolution of Localization

ANISSE ZEROUTA

a.zerouta@precogtec.com

Precog Technologies– Theoretical Physics Division https://orcid.org/0000-0001-7966-0746

Research Article

Keywords: scalar–aether gravity, dynamical memory, geometric charge, cosmological perturbations, localization, constrained Hamiltonian dynamics

Posted Date: September 30th, 2026

DOI: https://doi.org/10.21203/rs.3.rs-11203553/v1

License: This work is licensed under a Creative Commons Attribution 4.0 International License.
Read Full License

Additional Declarations: The authors declare no competing interests.

DJAMILAR: Geometric Charge and the Evolution of Localization

Memory, Cosmological Transport and a Finite Localization Budget

Anisse Zerouta

Theoretical Physics Division, Precog Technologies, Paris, France

a.zerouta@precogtec.com

29 September 2026

Abstract

Can one evolving geometric state generate a matter-like remnant and sustain intrinsic localization? We study this question in a covariant DJAMILAR extension in which material domains couple to a dynamical memory through their rest energy. The interaction produces a scalar charge, fixes a material force and permits relative charge transport. A positive produced dust-like term requires a positive scalar clock, so that at fixed aperture density the common aperture grows monotonically. For a constant-density size family, a localization scan obeys an exact Hill-curvature identity and a normalization-free null relation. For a positive population of domain sizes, the reduced charge-production profile is a convolution with a logistic kernel, implying one-sided variance and Fourier exclusion bounds; these are consistency conditions of principle, which require an independently reconstructed production history and a specified dynamical parameter point. Combining the opening history with the Gaussian localization law yields an exact weakening law and a finite future localization budget for any bounded normalization, while the same clock implies stronger past injection, linking the thermal and ionization history of diffuse gas to the accumulated aperture evolution. State-dependent rates can produce infinitely many increasingly weak transfers with finite accumulated decoherence, and the operational localization mass scales as the aperture to the power 18/7 in the reference regime. Independently, we derive a necessary and sufficient positivity criterion for the constrained scalar momentum block and its dust-like asymptotic restriction. These results assume a common homogeneous aperture and a prescribed test channel, without quantum backreaction or identification of a terrestrial opening with the cosmological one. Together, they make the coexistence of a geometric remnant and sustained localization a quantitative condition on the microscopic completion.

Keywords: scalar–aether gravity; dynamical memory; geometric charge; cosmological perturbations; localization; constrained Hamiltonian dynamics.

1 Introduction

A common geometric origin of a matter-like component and quantum localization imposes a joint requirement: the state which generates the remnant must also supply an admissible history for the localization channel. The abundance of the remnant and the ability to suppress spatial alternatives cannot be assigned independently once both depend on the same evolving aperture. This paper makes that requirement quantitative through a charge-producing action and a conditional connection to its quantum companion.

A contribution proportional to a^{-3} in a homogeneous energy density is suggestive of matter, but this scaling alone does not determine its spatial current, force on other constituents or

perturbations. Likewise, an instantaneous localization rate does not determine how much attenuation remains available over an evolving background. We calculate both distinctions in one specified architecture.

DJAMILAR proposes that a collective aperture state provides a common geometric description of gravitational response and quantum–classical behaviour. The original filtration proposal [1] was developed into a covariant scalar–aether–memory framework [2]; the latter explicitly replaces the original algebraic force law by action-derived dynamics. Two related Research Square preprints formulate localization and the reconstruction of its geometric kernel [3, 4]. They constrain the interpretation of a geometric response, but do not imply that loss of coherence becomes a conserved cosmological charge. That identification would require an additional microscopic derivation.

Related hybrid constructions have explored the converse direction in which stochastic localization or collapse events source a classical gravitational field [5], while recent work has emphasized diffusion and smearing as experimentally constraining ingredients in collapse and hybrid classical–quantum gravity [6]. These precedents motivate cross-sector consistency tests, but they do not supply the dynamical memory charge or the aperture evolution studied here.

Field-dependent particle masses and their cosmological forces have a substantial history, including dilaton-coupled matter [7], variable-mass dark matter [8], coupled quintessence [9], and interacting dark-sector models [10]. Our domain action belongs to this broad class at the continuum level. Its additional ingredients are the aperture-dependent interaction, dynamical memory and scalar–aether charge; the general idea of a scalar-dependent material mass is not a new claim.

The covariant gravitational representative is closely related to aether–scalar–tensor theory (AeST) [11]. Its temporal scalar sector already admits a dust-like contribution, and its constrained degrees of freedom and infrared behaviour require care [12, 13]. Consequently, neither the existence of such a contribution nor the need for Hamiltonian constraints is new here. Our question is more specific: can a dynamical memory produce this charge through an explicit interaction, and what else must happen if it does?

We introduce an effective rest-energy interaction per conserved material domain. Its geometric switching function is motivated by the aperture dependence in the DJAMILAR programme, while the interaction itself is an additional hypothesis. From this one choice we derive charge production, material recoil and charge transport. We then obtain an exact scalar momentum-positivity criterion on the active cosmological background, together with a late-time restriction and reproducible examples of the full linear response. The contribution is the joint structure of these results in the specified extension. We do not claim a model-independent origin of dark matter or priority for generic scalar-mediated attraction, Noether-charge sourcing or fluid actions.

The central cross-scale result is a finite future localization budget. A positive produced charge fixes the sign of the aperture evolution in the constant-density realization. If the same aperture controls a bounded-rate localization channel, even unlimited waiting supplies only finite additional attenuation. A second result distinguishes infinite event activity from unbounded resolving action. These statements do not assume that the remnant is all of dark matter or that the aperture has already been measured. They follow after the common-state and channel assumptions are made explicit in Section 4.

Production, retention, cold clustering and sustained localization are consequently separate requirements within a shared construction. The current and force identities, the localization budget, and the constrained scalar criterion specify how that construction can be tested or extended. The Gaussian channel and generic scalar-mediated forces are established ingredients; the contribution is the set of joint restrictions imposed by this realization.

The common-aperture connection has two logically different levels. The first is a laboratory statement: the assumed Hill activation imposes normalization-free relations between the slope

and curvature of a localization size scan. The second concerns the cosmological source. For a positive distribution of domain sizes, the reduced source must be a positive convolution of the same susceptibility kernel. This yields exclusion conditions on its width and low-frequency Fourier content only after the memory history and opening clock have been fixed by a specified dynamical parameter point and the reduced production profile has been reconstructed independently. We therefore treat these relations as consistency conditions, not as a present cosmological measurement of the switching exponent.

2 A covariant memory–domain extension

2.1 Fields, geometry and action

We use signature $(-,+,+,+)$ and $\hbar = c = 1$. The unit timelike aether is u^μ, with $u^\mu u_\mu = -1$. Define

$$\begin{aligned} h_{\mu\nu} &= g_{\mu\nu} + u_\mu u_\nu, & D_\mu\vartheta &= h_\mu{}^\nu \nabla_\nu \vartheta, \\ Y &= D_\mu\vartheta D^\mu\vartheta, & Q &= u^\mu\nabla_\mu\vartheta, \\ a^\mu &= u^\nu\nabla_\nu u^\mu, & \Theta &= \nabla_\mu u^\mu, & F_{\mu\nu} &= 2\nabla_{[\mu}u_{\nu]}. \end{aligned} \tag{1}$$

The aperture variable is dimensionless, $\vartheta = \ln(C_d/C_{d,\mathrm{ref}})$, with $C_d = \pi n_d r_d^2$. At fixed proper aperture density n_d, $r_d = r_{d,\mathrm{ref}} e^{\vartheta/2}$. The material-domain density introduced below is a different quantity.

Set $A = 2 - K_B$. The action studied here is

$$\begin{aligned} S = \frac{M_*^2}{2}\int \mathrm{d}^4x\sqrt{-g}\,[R - \tfrac{1}{2}K_B F_{\mu\nu}F^{\mu\nu} + 2Aa^\mu\nabla_\mu\vartheta - AY - A\mathcal{J}(Y) \\ + 2\mathcal{K}(Q) - \lambda(u^\mu u_\mu + 1)] \\ + \int \mathrm{d}^4x\sqrt{-g}\,[-\tfrac{1}{2}\nabla_\mu\Sigma\nabla^\mu\Sigma - \tfrac{1}{2}m_\Sigma^2\Sigma^2 - \gamma\nabla_\mu\Sigma(a^\mu - u^\mu\Theta)] - \sum_I \int \mu(\vartheta,\Sigma)\,\mathrm{d}\tau_I. \end{aligned} \tag{2}$$

We restrict to

$$\mathcal{K}(Q) = K_2(Q - Q_0)^2, \qquad \mathcal{J}(Y) = jY + O(Y^{3/2}), \qquad \mathcal{J}(0) = 0, \tag{3}$$

with constant $j > 0$, $K_2 > 0$ and $0 < K_B < 2$. The nonzero-Q_0 minimum is related to the construction of a timelike scalar condensate in ghost-condensation models [14]. The present scalar–aether spatial sector differs from the original ghost-condensate effective theory, so its higher-derivative dispersion and stability results cannot simply be imported. The $O(Y^{3/2})$ terms do not contribute to the quadratic action about a homogeneous scalar. We set the cosmological constant to zero in the dynamical model and all numerical runs; a separately labelled late-background matching estimate is discussed in Section 7. The field-dependent spatial constitutive law of more general representatives is not included in this restriction.

Each domain has bare mass $M_d > 0$ and effective mass

$$\mu = M_d + U, \qquad U(\vartheta,\Sigma) = \frac{E\Sigma^2}{f^2}F(\vartheta), \qquad F = \frac{1}{1 + e^{\beta(\vartheta - \vartheta_R)}}, \quad \beta = \frac{p}{2} > 0. \tag{4}$$

Here $E > 0$ is an energy and $f > 0$ a memory normalization. For a fixed proper domain radius R, $F = (R/r_d)^p/[1 + (R/r_d)^p]$, with $\vartheta_R = 2\ln(R/r_{d,\mathrm{ref}})$. This geometrical motivation uses two restrictions: fixed R and fixed n_d. Domain formation, mergers and varying aperture density are outside the model. The existing domain mass appears once, in the last term of (2); it is not added again as a separate dust action.

In mass dimensions, $[\Sigma] = [f] = [\gamma] = [m_\Sigma] = [Q_0] = [E] = 1$, $[M_*^2] = 2$, $[n] = 3$, and $[K_2] = [K_B] = [j] = [\vartheta] = 0$. Thus $[U] = 1$ and $[nU] = 4$. Equation (4) is an effective interaction assumption, not a derivation from the quantum localization generator. It is an additional hypothesis; exact consequences within this model retain that conditional status.

2.2 Current, material force and memory equation

Varying ϑ gives

$$I^\mu = M_*^2\big[Aa^\mu - A(1+\mathcal{J}_Y)D^\mu\vartheta + \mathcal{K}_Q u^\mu\big], \qquad \nabla_\mu I^\mu = -nU_\vartheta, \tag{5}$$

where n is the proper number density of domains in the continuum limit. Their four-velocity v_d^μ obeys

$$\nabla_\mu(nv_d^\mu) = 0, \tag{6}$$

$$v_d^\nu\nabla_\nu v_d^\mu = -(g^{\mu\nu} + v_d^\mu v_d^\nu)\nabla_\nu \ln\mu. \tag{7}$$

These equations follow by variation of the variable-mass worldlines. A continuum description using material labels preserves number conservation and the metric constraints [15, 16].

The memory equation in the present restriction is

$$\Box\Sigma - m_\Sigma^2\Sigma - nU_\Sigma + \gamma\nabla_\mu(a^\mu - u^\mu\Theta) = 0. \tag{8}$$

For the switching function in (4),

$$U_\vartheta = -\frac{E\beta\Sigma^2}{f^2}F(1-F), \qquad U_\Sigma = \frac{2E\Sigma}{f^2}F. \tag{9}$$

The same interaction therefore fixes the charge source and the force. Dropping (7) while retaining charge production would change the model and violate its action-based closure.

3 Homogeneous production and the remnant charge

For a spatially flat FLRW background with aligned aether and domain flow, $Q = \dot\vartheta$, $n = n_0/a^3$. Define

$$C_Q = a^3\mathcal{K}_Q, \qquad Q = Q_0 + \frac{C_Q}{2K_2a^3}. \tag{10}$$

The source equation becomes

$$\dot{C_Q} = -\frac{n_0}{M_*^2}U_\vartheta = \frac{n_0E\beta}{M_*^2f^2}\Sigma^2F(1-F) \geq 0. \tag{11}$$

This is monotonic charge production for the stated interaction. It is not monotonic energy creation. The scalar contribution is

$$\rho_Q = M_*^2\left(\frac{Q_0C_Q}{a^3} + \frac{{C_Q}^2}{4K_2a^6}\right), \qquad p_Q = \frac{M_*^2{C_Q}^2}{4K_2a^6}. \tag{12}$$

For $Q_0 > 0$ and an initially nonnegative charge, the first term is positive and becomes dust-like when the a^{-6} term is small. Its normalization is a dynamical integral of the history of Σ and F, not a fixed universal constant.

Writing $v = \dot{\Sigma}$, the remaining background expressions are

$$\rho_\Sigma = \tfrac{1}{2}v^2 + \tfrac{1}{2}m_\Sigma^2\Sigma^2 + 3\gamma H v, \qquad p_\Sigma = \tfrac{1}{2}v^2 - \tfrac{1}{2}m_\Sigma^2\Sigma^2 - \gamma\dot{v}, \tag{13}$$

$$\rho_d = n\mu, \qquad p_d = 0, \tag{14}$$

$$3M_*^2H^2 = \rho_Q + \rho_\Sigma + \rho_d, \tag{15}$$

$$\dot{v} + 3Hv + m_\Sigma^2\Sigma + nU_\Sigma + 3\gamma(\dot{H} + 3H^2) = 0. \tag{16}$$

The apparently implicit derivatives in these equations are regular. With

$$\begin{aligned} \mathcal{A}_b &= \rho_d + M_*^2 Q C_Q/a^3 + v^2 + 3\gamma H v, \\ \mathcal{B}_b &= 3Hv + m_\Sigma^2\Sigma + nU_\Sigma + 9\gamma H^2, \end{aligned} \tag{17}$$

we have

$$\dot{H} = -\frac{\mathcal{A}_b + \gamma\mathcal{B}_b}{2M_*^2 + 3\gamma^2}, \qquad \dot{v} = \frac{3\gamma\mathcal{A}_b - 2M_*^2\mathcal{B}_b}{2M_*^2 + 3\gamma^2}. \tag{18}$$

The energy exchanges provide a useful independent sign check:

$$\begin{aligned} \dot{\rho}_Q + 3H(\rho_Q + p_Q) &= -nQU_\vartheta, \\ \dot{\rho}_d + 3H\rho_d &= n(QU_\vartheta + vU_\Sigma), \\ \dot{\rho}_\Sigma + 3H(\rho_\Sigma + p_\Sigma) &= -nvU_\Sigma. \end{aligned} \tag{19}$$

Their sum vanishes. No energy reservoir can be counted twice by interpreting the charge as geometry.

3.1 Curvature can initiate memory and charge

For $\Sigma_i = v_i = C_{Q_i} = 0$ and nonzero dust density, (18) implies

$$\ddot{\Sigma}_i = -\frac{9\gamma M_*^2 H_i^2}{2M_*^2 + 3\gamma^2}. \tag{20}$$

An initially vanishing memory is therefore not preserved when $\gamma \neq 0$. Expanding $\Sigma = \ddot{\Sigma}_i(t - t_i)^2/2 + \cdots$ in (11) gives

$$C_Q(t) = \frac{n_0 E p F_i(1 - F_i)}{40M_*^2 f^2}\ddot{\Sigma}_i^2(t - t_i)^5 + O((t - t_i)^6). \tag{21}$$

This delayed onset is a definite prediction of the conditional model. Its coefficient vanishes for $\gamma = 0$, $E = 0$, or a fully closed switching window. It does not predict an observed abundance without a physical normalization and cosmological initial conditions.

3.2 A restriction on positive production pulses

One might try to replace the monotonic switch by a compact interaction pulse without changing the sign of production. Consider more generally $U = \Sigma^2 u(\vartheta)$, with $u \geq 0$. If $\dot{C}_Q \geq 0$ is required for every allowed memory history, then $u' \leq 0$. If also $u(-\infty) = u(+\infty) = 0$, monotonicity forces $u \equiv 0$. A nontrivial interaction which vanishes on both sides cannot guarantee instantaneous positive production for all histories under these assumptions. Positive *net* production can still occur with a source of changing sign weighted by a nontrivial memory history. The logistic interaction avoids this obstruction by approaching a nonzero u at one end; it is not a compact pulse.

4 Positive charge and a finite localization budget

The same aperture state enters a second physical question: how much localization can its subsequent evolution supply? This section connects the charge-producing representative to the Gaussian localization law of the quantum companions [3, 4]. The connection is an additional common-state assumption, not a derivation of that quantum law from the classical action. It leads to a finite-exposure theorem and specifies the state dependence required to evade it.

4.1 The common-state assumption and the opening clock

Consider a homogeneous patch in which the localization aperture follows the scalar background, with fixed proper aperture density n_d. For a produced charge $C_Q > 0$, positivity of its dust-like contribution requires $Q_0 > 0$. Equation (11) and $K_2 > 0$ then imply

$$Q = Q_0 + \frac{C_Q}{2K_2 a^3} \geq Q_0 > 0, \qquad \frac{\mathrm{d}\ln r_d}{\mathrm{d}t} = \frac{Q}{2}. \tag{22}$$

In particular, for $r_i = r_d(t_i)$,

$$\ln\frac{r_d(t)}{r_i} = \frac{Q_0}{2}(t - t_i) + \frac{1}{4K_2}\int_{t_i}^{t} \frac{C_Q(t')}{a(t')^3}\,\mathrm{d}t'. \tag{23}$$

This exact identity holds during production as well as after it. A geometrical crossing $r_d = R$ maximizes $F(1-F)$, but need not maximize the full source $\Sigma^2 F(1-F)$. It cannot be identified with the end of production without solving the memory history.

For later use, Eqs. (12) and (22) also give

$$\rho_Q = M_*^2 K_2 (Q^2 - Q_0^2), \qquad p_Q = M_*^2 K_2 (Q - Q_0)^2, \qquad \frac{Q}{Q_0} = \frac{1 + w_Q}{1 - w_Q}, \quad w_Q \equiv \frac{p_Q}{\rho_Q}. \tag{24}$$

Thus the equation-of-state ratio fixes only Q/Q_0; the absolute clock scale Q_0 remains part of the cosmological normalization.

Let a fixed rigid test domain have mass M and radius R_{q}, which need not equal the radius of the charge-producing domains. The quantum realization specifies

$$\Gamma_D(t) = \gamma_{\mathrm{loc}}(t)\left(\frac{M}{m_0}\right)^{\alpha} F_{\mathrm{q}}(t), \qquad F_{\mathrm{q}} = \frac{1}{1 + (r_d/R_{\mathrm{q}})^p}, \tag{25}$$

$$\mathcal{R}_D(d,t) = \Gamma_D(t)(1 - e^{-\xi}), \qquad \xi = \frac{d^2}{4r_d^2}, \tag{26}$$

where $p, \alpha > 0$, m_0 is a reference mass and $d > 0$ is a fixed physical separation. The bare rate γ_{loc} is distinct from the derivative coupling γ in the classical action. Momentum-transfer descriptions of decoherence and their relation to jump processes are established [17]; neither the Gaussian channel nor that relation is a novelty claim here. The new restriction follows from imposing (22) on this aperture-dependent channel.

We use its time-dependent, local Markov realization on the prescribed background. For two held alternatives, or the channel contribution along specified paths of fixed separation, the attenuation exponent is

$$\mathcal{B}(t_i, t; d) = \int_{t_i}^{t} \mathcal{R}_D(d, t')\,\mathrm{d}t', \qquad \frac{V_D(t)}{V_D(t_i)} = e^{-\mathcal{B}(t_i,t;d)}. \tag{27}$$

Other environmental channels and uncontrolled free-wavepacket spreading are not included in this expression. The rigid-domain requirement is $\sigma_{\mathrm{rel}} \ll r_d$, together with mechanical integrity

over the interval considered. A slowly varying aperture over each laboratory protocol is sufficient for the local use of (25); a microscopic derivation of its evolving noise spectrum is still needed.

This construction does not set the present cosmological aperture equal to a terrestrial value. The 25 nm value used in the companion examples is a benchmark, not a measured cosmological boundary condition. A local experiment requires the matching problem described in Refs. [3, 4]. The results below do not use that numerical value or a dark-matter abundance identification.

4.2 Laboratory susceptibility and positive-population consistency bounds

The common-state assumption has a laboratory consequence that can be tested before any cosmological interpretation. Consider a constant-density family of rigid domains, $M \propto R^3$, at fixed geometric state and with a size-independent bare normalization. For the Hill activation

$$F_p(z) = \frac{z^p}{1+z^p}, \qquad z = \frac{R}{r_d}, \tag{28}$$

the size-dependent rate is $\Gamma_D \propto R^{3\alpha} F_p(R/r_d)$. Define

$$S(R) = \frac{\mathrm{d}\ln\Gamma_D}{\mathrm{d}\ln R}, \qquad \kappa(R) = -\frac{\mathrm{d}^2\ln\Gamma_D}{\mathrm{d}(\ln R)^2}. \tag{29}$$

Direct differentiation gives

$$S = 3\alpha + p(1-F_p), \qquad \kappa = p^2 F_p(1-F_p), \tag{30}$$

and hence the normalization-free null relation

$$\boxed{\kappa = (S-3\alpha)(3\alpha+p-S).} \tag{31}$$

Equation (31) is a laboratory consistency test of the Hill switching law. It does not use the memory amplitude, charge abundance or cosmological opening clock; a significant violation rejects this activation model even if a crossover length can be fitted.

A weaker cosmological consequence follows if the same switch is retained for several conserved domain species. Let $x = \ln R$, $s = \ln r_d$, and let $\mathcal{W}(x) \geq 0$ denote their comoving interaction weight. The normalized susceptibility kernel is

$$P_p(y) = \frac{\mathrm{d}F_p}{\mathrm{d}y} = \frac{p}{4}\,\mathrm{sech}^2\!\left(\frac{py}{2}\right), \qquad \int_{-\infty}^{\infty} P_p(y)\,\mathrm{d}y = 1. \tag{32}$$

The reduced production profile is then

$$\mathcal{S}(s) \equiv \frac{2M_*^2 f^2}{\Sigma^2}\dot{C}_Q = \int_{-\infty}^{\infty} \mathcal{W}(x) P_p(x-s)\,\mathrm{d}x. \tag{33}$$

After normalization, $w = \mathcal{W}/\int \mathcal{W}\mathrm{d}x$ and $j = \mathcal{S}/\int \mathcal{S}\mathrm{d}s$ obey $j = w * P_p$. Since

$$\widehat{P}_p(k) = \frac{\pi k/p}{\sinh(\pi k/p)}, \tag{34}$$

positivity of w implies the one-sided Fourier envelope

$$\boxed{|\widehat{j}(k)| \leq \frac{\pi|k|/p}{\sinh(\pi|k|/p)}} \tag{35}$$

and the variance bound

$$\boxed{\mathrm{Var}(j) = \mathrm{Var}(w) + \frac{\pi^2}{3p^2} \geq \frac{\pi^2}{3p^2}.} \tag{36}$$

A laboratory value $p_{\rm lab}$ therefore supplies an exclusion bound, not a cosmological estimator of p: a reduced profile narrower than $\pi/(\sqrt{3}\,p_{\rm lab})$, or a low-frequency Fourier amplitude above (35), is incompatible with a positive conserved population in this realization. A broader profile does not determine p, because the unknown population can add positive broadening.

The scope of these inequalities is important. They constrain $\dot{C}_Q/\Sigma^2$, not an arbitrary physical source history. They become empirical tests only if a future observable reconstructs the reduced production profile independently and a specified parameter point fixes both $\Sigma(t)$ and the absolute opening clock $Q(t)$. The memory equation itself contains the population-dependent loading

$$\Delta\Omega^2_{\Sigma,\mathcal{W}}(t) = \frac{2}{a^3(t)f^2}\int_{-\infty}^{\infty}\mathcal{W}(x)F_p[x-s(t)]\,\mathrm{d}x. \tag{37}$$

If the bounds are to remain independent of the unknown population, we therefore restrict to a weak-loading regime

$$\Delta\Omega^2_{\Sigma,\mathcal{W}} \ll m^2_\Sigma. \tag{38}$$

Outside this regime there is no logical circularity, but $\mathcal{W}$ and Σ must be inferred jointly from the coupled dynamics, so the simple population-independent closure is lost. Likewise, converting the size-space bound to time requires the absolute clock: for nearly constant Q, $\sigma_t Q \geq 2\pi/(\sqrt{3}\,p)$, while Eq. (24) fixes only Q/Q_0. No cosmological production-history reconstruction is performed in this paper. The complete positive-population deconvolution criterion is given in Appendix C.

4.3 Monotonic weakening and finite total future exposure

For constant positive $\gamma_{\rm loc}$, differentiation at fixed $M, R_{\rm q}, d$ gives the exact law

$$\boxed{\frac{\mathrm{d}\ln\mathcal{R}_D}{\mathrm{d}t} = -\frac{Q}{2}\left[p(1-F_{\rm q}) + \frac{2\xi}{e^\xi-1}\right] < 0.} \tag{39}$$

Both activation and resolving power weaken as the opening grows. When $r_d \gg R_{\rm q}, d$,

$$\mathcal{R}_D \simeq \frac{\gamma_{\rm loc}}{4}\left(\frac{M}{m_0}\right)^\alpha \frac{R_{\rm q}^p d^2}{r_d^{p+2}}. \tag{40}$$

If $Q \to Q_0$, its dominant exponential is $\exp[-(p+2)Q_0 t/2 + o(t)]$. For $p=4$ this is $\exp[-3Q_0 t + o(t)]$. A stronger result does not require $Q \to Q_0$ or an assumed expansion law.

Proposition 1 (Finite future localization budget)**.** *Suppose a future-complete background and a fixed test domain obey (22), with $Q_0 > 0$, $p > 0$, and $0 \leq \gamma_{\rm loc}(t) \leq \bar{\gamma} < \infty$. If the specified quantum channel remains applicable, put $\Gamma_* = \bar{\gamma}(M/m_0)^\alpha$. Its integrated future jump intensity and fixed-separation attenuation satisfy*

$$N_{D,\infty} \equiv \int_{t_i}^{\infty}\Gamma_D\,\mathrm{d}t \leq \frac{2\Gamma_*}{pQ_0}\ln\left[1+\left(\frac{R_{\rm q}}{r_i}\right)^p\right] < \infty, \tag{41}$$

$$\mathcal{B}_\infty(d) \leq \min\left\{\frac{2\Gamma_*}{pQ_0}\ln\left[1+\left(\frac{R_{\rm q}}{r_i}\right)^p\right], \frac{\Gamma_*}{2(p+2)Q_0}\left(\frac{R_{\rm q}}{r_i}\right)^p\left(\frac{d}{r_i}\right)^2\right\}. \tag{42}$$

Proof. The opening is monotonic and $\mathrm{d}t \leq 2\mathrm{d}r_d/(Q_0 r_d)$. Hence

$$N_{D,\infty} \leq \frac{2\Gamma_*}{Q_0}\int_{r_i}^{\infty}\frac{\mathrm{d}r}{r[1+(r/R_{\rm q})^p]}, \tag{43}$$

which evaluates to (41). For attenuation, use $1-e^{-\xi} \leq 1$ to obtain the first bound. The inequalities $F_{\rm q} \leq (R_{\rm q}/r)^p$ and $1-e^{-\xi} \leq d^2/(4r^2)$ give the second after integrating $r^{-(p+3)}$. All bounds are dimensionless. □

Thus the channel has a finite remaining ability to suppress new alternatives. If an attenuation target $\chi = -\ln \epsilon > 0$ exceeds the bound in (42), no extension of the waiting time can achieve it through this channel on that history. For the held alternatives in (27), a nonzero initial coherence has a strictly positive channel multiplier $e^{-\mathcal{B}_\infty}$. That multiplier may nevertheless be extraordinarily small. The result does not restore coherence previously lost, and it does not preclude classical behaviour produced by other channels or by an already sufficient finite suppression. It identifies an incompatibility between the stated background/channel assumptions and an arbitrarily large remaining attenuation for the fixed domain.

The event statement refers to the specified jump representation. It is not a count of observed microscopic geometric events or a proof of individual measurement outcomes. The distinction between ensemble decoherence and a complete collapse interpretation remains essential [18].

4.4 A moving mass threshold, including unlimited waiting

Consider a family with fixed material density ρ_m, $M = c_\rho R_{\mathrm{q}}^3$, $c_\rho = 4\pi\rho_m/3$, and a fixed separation d, short exposure T, and target χ. During each exposure take the background as stationary. The equation $\mathcal{R}_D T = \chi$ defines a unique positive critical radius R_c because the rate grows strictly with R_{q} for $\alpha > 0$. At constant γ_{loc} its exact state slope is

$$\frac{\mathrm{d}\ln R_c}{\mathrm{d}\ln r_d} = \frac{p(1-F_c) + 2\xi/(e^\xi - 1)}{3\alpha + p(1-F_c)} > 0. \tag{44}$$

For $R_c, d \ll r_d$, this becomes

$$R_c \propto r_d^{(p+2)/(3\alpha+p)}, \qquad M_c \propto r_d^{3(p+2)/(3\alpha+p)}. \tag{45}$$

At $\alpha = 1, p = 4$, the powers are $6/7$ and $18/7$: doubling the aperture multiplies the operational mass threshold by $2^{18/7} \simeq 5.94$. These powers assume fixed d, T, ρ_m; a Talbot exposure or a separation that scales with size gives a different protocol-dependent relation.

Proposition 1 also gives a necessary size condition when the waiting time is unlimited. Using its second bound, reaching χ requires

$$R_{\mathrm{q}} \geq \left[\frac{2(p+2)Q_0\chi\, r_i^{p+2}}{\bar{\gamma}(c_\rho/m_0)^\alpha d^2}\right]^{1/(3\alpha+p)}. \tag{46}$$

This is a necessary condition, not a sufficient localization criterion: the bound need not be saturated. It depends on the separation, background opening and rate ceiling, so it is not a universal mass dividing quantum and classical matter. Its distinctive feature is the absence of an adjustable exposure time.

4.5 Infinite event activity can coexist with finite decoherence

A state-dependent normalization can change the conclusion. To classify a controlled family, suppose $Q \to Q_0 > 0$ and

$$\gamma_{\mathrm{loc}}(t) = \gamma_i \left[\frac{r_d(t)}{r_i}\right]^{b_\gamma}. \tag{47}$$

For the same fixed domain and separation, the late rates scale as

$$\Gamma_D \propto r_d^{b_\gamma - p}, \qquad \mathcal{R}_D \propto r_d^{b_\gamma - p - 2}. \tag{48}$$

The asymptotically positive constant opening rate makes their time integrals converge or diverge as follows:

Normalization exponent	$N_{D,\infty}$	$\mathcal{B}_\infty(d)$
$b_\gamma < p$	finite	finite
$p \le b_\gamma < p+2$	infinite	finite
$b_\gamma \ge p+2$	infinite	infinite

The middle regime is physically informative: infinitely many increasingly weak transfers do not guarantee unbounded resolving action at a fixed physical separation. At $p = 4$, the thresholds are $b_\gamma = 4$ for event activity and $b_\gamma = 6$ for accumulated decoherence. The choice $b_\gamma = 2$ leaves both integrals finite. A bounded normalization therefore cannot maintain a nonzero late localization rate in this branch; within the power-law family, $b_\gamma = 6$ is the marginal compensation for a constant late rate. The normalization itself is not predicted by the classical action.

4.6 A charge-carrying background and reproducible example

The bounds do not require a background fit. For a check on an exact classical solution, set $\gamma = \Sigma = \dot{\Sigma} = 0$, keep $C_Q > 0$ constant, and set $a(t_i) = 1$. This invariant subspace has $U = 0$ and

$$\rho_{m,i} = \rho_{d,i} + M_*^2 Q_0 C_Q, \qquad \rho_{s,i} = \frac{M_*^2 {C_Q}^2}{4K_2}, \qquad a^3 = 1 + 3H_i\Delta t + \frac{3\rho_{m,i}}{4M_*^2}\Delta t^2, \tag{49}$$

with $3M_*^2 H_i^2 = \rho_{m,i} + \rho_{s,i}$ and $\Delta t = t - t_i$. The opening follows (23). The initial charge is an input on this branch, not a newly calculated production history.

Use the dimensionless values $M_*^2 = Q_0 = K_2 = 1$, $C_Q = 0.2$, $\rho_{d,i} = 0.1$ and $r_i = R_\mathrm{q} = d = 1$. With $g = \gamma_i (M/m_0)^\alpha / Q_0$, direct integration for constant normalization gives

$$N_{D,\infty}/g = 0.324602, \qquad \mathcal{B}_\infty/g = 0.0457076. \tag{50}$$

The event bound is $0.346574g$. Integrating the resolving kernel on the limiting clock $\ln \dot{r}_d = Q_0/2$ gives the tighter envelope $\mathcal{B}_\infty \le 0.0491500g$, while the elementary second bound in (42) is $g/12$. The limiting clock is used as a bound, not as an exact nonzero-charge solution.

For $b_\gamma = 4$, one instead finds $\mathcal{B}_\infty/g = 0.176939$, although N_D/g grows asymptotically linearly in $Q_0\Delta t$. For $b_\gamma = 6$, the late resolving rate tends to $gQ_0/4$ and its integrated effect diverges. Figure 1 displays these alternatives. The script `check_localization_budget.py` checks the exact derivatives, compares the background with an independent ODE integration, and compares exposure quadrature with cumulative evolution. The maximum Friedmann residual is 2.0×10^{-16}, and the analytic/ODE log-aperture difference is below 8.0×10^{-13} in this benchmark.

4.7 What a common microscopic completion must supply

For this nondissipative Gaussian channel, restoring $\hbar$, the energy-injection rate is $\dot{E}_D = 3\hbar^2\Gamma_D/(4Mr_d^2)$ [3]. Since $1 - e^{-\xi} \le \xi$, a fixed separation obeys

$$\mathcal{B}(t_i, t; d) \le \frac{Md^2}{3\hbar^2} \int_{t_i}^{t} \dot{E}_D \, \mathrm{d}t'. \tag{51}$$

Thus the compensation $b_\gamma \ge p + 2$ entails an unbounded total supplied energy over an infinite future within this channel. This is an injection statement, not a claim that cosmological thermal energy must grow without cooling. Dissipative collapse dynamics provides explicit alternatives to unrestricted energy growth [19]; such a completion changes the noise/friction structure and must be derived rather than assumed to preserve all of the present identities.

Changing the geometrical clock is another distinct possibility. If n_d evolves, the exact identity is $2\ln \dot{r}_d = Q - \ln \dot{n}_d$. Holding the homogeneous aperture fixed while $Q > 0$ requires $\ln \dot{n}_d = Q$.

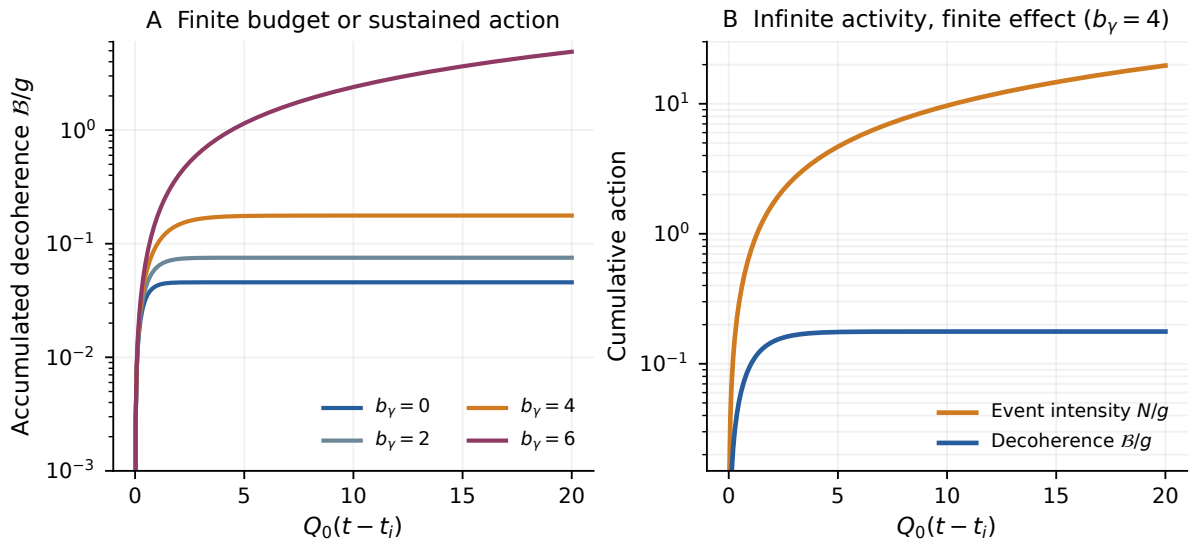


Figure 1: Future resolving action of a prescribed quantum test channel on the exact classical background (49). All curves use $p = 4$, $r_i = R_{\rm q} = d = 1$, and are divided by g. Panel A distinguishes finite attenuation budgets from sustained action as the normalization exponent b_γ changes. Panel B shows that, at $b_\gamma = 4$, event intensity grows without bound while attenuation approaches a finite limit. The infinite-time statements follow from the derived asymptotics, not from the plotted finite interval. The example has no observational calibration and includes no quantum heating backreaction.

Alternatively, a material region may not track the homogeneous state. Both possibilities require a microscopic evolution or a local matching solution absent from the fixed-n_d restriction. A constant-aperture channel with nonzero fixed rate is a direct counterexample to the finite-budget conclusion when that clock assumption is removed.

The quantum channel in this section is a test-sector extension: its fluctuating reservoir and stress-energy backreaction have not been added to (2). The exact classical solution and the localization calculation must not be confused with a self-consistent quantum-cosmological solution. The infrared consistency question analysed below is also not resolved by the finite-budget theorem. Subject to these declared premises, the connection is nevertheless restrictive: the same sign of charge that supports a positive remnant determines an opening history, which bounds the future localization available from a bounded-rate common-aperture channel.

4.8 Past aperture evolution and the thermal history of diffuse gas

The same opening clock has a retrospective consequence that can connect the construction to observations. On an expanding homogeneous branch, define the dimensionless accumulated evolution between redshift z and the present by

$$W(z) = \int_{t(z)}^{t_0} Q(t)\,\mathrm{d}t, \qquad r_d(z) = r_{d0} e^{-W(z)/2}. \tag{52}$$

Here r_{d0} is a cosmological parameter; it need not equal a terrestrial aperture. For a fixed domain to which the Gaussian channel applies, its exact kinetic-energy injection is

$$\dot{E}_D(z) = \frac{3\hbar^2}{4M}\left(\frac{M}{m_0}\right)^{\alpha} \frac{\gamma_{\rm loc}(z)}{r_d(z)^2[1 + (r_d(z)/R_{\rm q})^p]}. \tag{53}$$

At constant normalization this increases towards the past while $Q > 0$. If both epochs lie in $r_d \gg R_{\rm q}$, its ratio to the present value is approximately $\exp[(p+2)W/2]$, or e^{3W} for $p = 4$. This

scaling must not be extrapolated through activation saturation: at $r_d \ll R_{\rm q}$, heating scales instead as r_d^{-2}. The fixed-separation localization rate also saturates once $r_d \ll R_{\rm q}, d$. The channel and rigid-domain approximation must remain valid throughout the interval.

Diffuse neutral gas provides a candidate cosmological application without imposing laboratory–background equality. Homogeneity alone, however, does not establish the appropriate atomic domain or its noise coupling. If the injected energy populates isotropic translational motion of nonrelativistic particles of fixed composition, its temperature-source term is $2\dot{E}_D/(3k_B)$ per particle. Expansion cooling, Compton exchange, other heating and cooling, and changes of ionization must then be evolved together. The Thomson optical depth over a specified redshift interval is

$$\tau(z_1, z_2) = c\sigma_T \int_{z_1}^{z_2} \frac{n_e(z)}{(1+z)H(z)}\,\mathrm{d}z, \tag{54}$$

where n_e is the proper free-electron density. Planck constrains reionization through this quantity and the CMB spectra [20]; a heating law cannot be converted directly into an optical-depth bound without calculating the ionization response.

Unlike the future-budget theorem, an observational upper bound on past geometric evolution requires a specified normalization history or an independently justified positive lower bound on it. A rate ceiling alone allows negligible past injection. In particular, a lower rate inferred from a chosen laboratory classicality target cannot be imposed on the cosmological gas without an additional universality assumption. With these inputs, thermal and ionization data can constrain the history $W(z)$ jointly with r_{d0} and the rate parameters. They do not generically constrain only the endpoint $W(z_{\rm rec})$, since the timing of injection and cooling matters. Equations (52)–(54) therefore supply an observational route to the accumulated aperture evolution, without a dark-matter abundance identification. No numerical thermal exclusion is claimed here.

5 Why charge production does not determine clustering

5.1 An exact balance along material worldlines

Decompose the current relative to the material flow:

$$q_d = -v_{d\mu} I^\mu, \qquad j_d^\mu = I^\mu - q_d v_d^\mu, \qquad \kappa = \frac{q_d}{n}. \tag{55}$$

Using (6) and (5) yields

$$\boxed{v_d^\mu \nabla_\mu \kappa = -U_\vartheta - \frac{1}{n}\nabla_\mu j_d^\mu.} \tag{56}$$

This is an exact covariant identity. The charge per material domain changes through both local production and the divergence of a relative flux. After the source vanishes, the total charge on an appropriate closed or no-flux region is conserved; κ need not be constant along each domain. The geometric component and the material carrier can develop different spatial distributions.

The identity supplies an inverse diagnostic as well: if a material flow, a charge-per-domain field and the local source were determined, their discrepancy would reconstruct $\nabla_\mu j_d^\mu$. It does not reconstruct the complete vector current, since divergence-free contributions remain undetermined. Establishing an observational map to these quantities requires the full metric and matter solution.

5.2 A relation between memory response and material attraction

At fixed local background define

$$\Omega_\Sigma^2 = m_\Sigma^2 + nU_{\Sigma\Sigma} = m_\Sigma^2 + \frac{2nEF}{f^2}, \qquad \mathcal{A}_\Sigma = \frac{nU_\Sigma^2}{\mu}. \tag{57}$$

The chosen quadratic memory interaction gives the exact identity

$$\boxed{\mathcal{A}_\Sigma = 2(\Omega_\Sigma^2 - m_\Sigma^2)\frac{U}{M_d + U}.} \tag{58}$$

Both sides have dimension mass squared. The effective memory frequency and material attraction cannot be specified independently. The fractional loading $U/(M_d + U)$ and the frequency shift provide a more informative characterization than E alone.

The same separable interaction gives a second internal consistency relation. Since $U(\vartheta, \Sigma) = \Sigma^2 g(\vartheta)$ in the present representative, the homogeneous source and the memory-frequency loading obey

$$\boxed{\frac{\dot{C}_Q}{\Sigma^2} = -\frac{1}{4M_*^2}\frac{\partial}{\partial \ln r_d}\left[a^3(\Omega_\Sigma^2 - m_\Sigma^2)\right].} \tag{59}$$

This identity is structural rather than a test of the Hill form or of the quantum common-switch hypothesis: it follows from the separability $U = \Sigma^2 g(\vartheta)$ and should be read together with (58).

To identify the sign of the feedback, freeze the coefficients, neglect expansion and the metric–aether–ϑ response, and retain a cold domain density perturbation δ_n and a memory perturbation s. The local subsystem is

$$\ddot{s} + (q^2 + \Omega_\Sigma^2)s + nU_\Sigma \delta_n = 0, \qquad \ddot{\delta}_n + \frac{U_\Sigma}{\mu}q^2 s = 0. \tag{60}$$

An exponential solution $e^{\lambda t}$ satisfies

$$\lambda^2(\lambda^2 + q^2 + \Omega_\Sigma^2) - \mathcal{A}_\Sigma q^2 = 0, \tag{61}$$

so that

$$\lambda_+^2 = \frac{-(q^2 + \Omega_\Sigma^2) + \sqrt{(q^2 + \Omega_\Sigma^2)^2 + 4\mathcal{A}_\Sigma q^2}}{2} > 0 \tag{62}$$

when $U_\Sigma \neq 0$ and $q > 0$. This is attractive feedback, not a new generic scalar-force phenomenon; related instabilities occur in coupled scalar–matter models [21]. Here its coefficient is tied to the charge-producing interaction by (58).

For $q \ll \Omega_\Sigma$, $\lambda_+^2 \simeq \mathcal{A}_\Sigma q^2/\Omega_\Sigma^2$; for $q \gg \Omega_\Sigma$, it tends to $\mathcal{A}_\Sigma$. These limits refer only to the frozen subsystem. An oscillating Σ, expansion, other scalar modes and an effective-theory cutoff can invalidate an integrated frozen growth estimate. Our numerical results below use the full constrained scalar system instead.

A useful separation already follows without that approximation. Production contains $F(1-F)$, whereas the force coefficient contains F and Σ. For $F \simeq 1$ and an excited memory, production can be suppressed while attraction remains substantial. After $F \to 0$, the interaction force switches off but the intrinsic spatial current in (5) remains. This explains why stopping production neither certifies harmless earlier dynamics nor freezes the final distribution.

6 Constrained scalar dynamics on the active background

We consider scalar Fourier modes with $q = k/a > 0$. In aether-normal time gauge and spatial gauge $E_{\mathrm{metric}} = 0$, write

$$N = 1 + \phi, \qquad h_{ij} = a^2 e^{2\zeta}\delta_{ij}, \qquad N^i = a^{-2}\partial^i B, \qquad \nu = \frac{\Delta B}{a^2}. \tag{63}$$

Thus $B = -\nu/q^2$ for a Fourier mode. Set $\chi = \delta\vartheta$ and $s = \delta\Sigma$. Conserved domain labels $X^I = x^I + \partial^I\pi$ give $\delta_N = \Delta\pi$ and the proper number contrast

$$\delta_n = \frac{\delta n}{n} = \delta_N - 3\zeta. \tag{64}$$

The four scalar coordinates are $x = (\zeta, \chi, s, \delta_N)^T$. The longitudinal aether degree of freedom is encoded in the gauge-fixed scalar geometry, not discarded. The use of the normal aether is restricted to this quadratic scalar sector about the aligned background; it is not an identification of the general nonlinear vector theory with a hypersurface-orthogonal theory.

The complete quadratic Lagrangian is displayed in Appendix A. Let $\mathcal{L}_2$ be the Lagrangian divided by a^3, and let $P = \partial\mathcal{L}_2/\partial\dot{x}$ be the similarly normalized momentum. The actual canonical momentum is a^3P. Its velocity Hessian is

$$G_4 = \begin{pmatrix} -6M_*^2 & 0 & 3\gamma & 0 \\ 0 & 2M_*^2K_2 & 0 & 0 \\ 3\gamma & 0 & 1 & 0 \\ 0 & 0 & 0 & \rho_d/q^2 \end{pmatrix}. \tag{65}$$

Legendre transformation before constraint elimination yields the remarkably simple constraint block

$$\mathcal{H}_{cc} = \mathrm{diag}(-M_*^2K_Bq^2, -2M_*^2/3), \qquad c = (\phi, \nu). \tag{66}$$

It is invertible for the assumptions made here. The lapse and shift can therefore be eliminated without a quasistatic approximation or a division by a background-dependent kinetic eigenvalue.

For completeness, define $\Pi = (-6M_*^2H + 3\gamma v, M_*^2\mathcal{K}_Q, v + 3\gamma H)$ and

$$f_0 = -3M_*^2H^2 + M_*^2K_2(Q - Q_0)^2 + \tfrac{1}{2}v^2 - \tfrac{1}{2}m_\Sigma^2\Sigma^2 + 3\gamma Hv. \tag{67}$$

The constraint solutions are $\phi = C_\phi/(M_*^2K_Bq^2)$ and $\nu = 3C_\nu/(2M_*^2)$, where

$$\begin{aligned} C_\phi &= HP_\zeta + QP_\chi + vP_s - (3f_0 + 2M_*^2q^2)\zeta \\ &\quad + (nU_\vartheta - M_*^2Aq^2)\chi + (m_\Sigma^2\Sigma + \gamma q^2 + nU_\Sigma)s + \rho_d\delta_N, \end{aligned} \tag{68}$$

$$C_\nu = P_\zeta/3 + P_{\delta_N} - \Pi\cdot(\zeta, \chi, s). \tag{69}$$

The reduced Hamiltonian density per a^3 is

$$\mathcal{H}_{\mathrm{red}} = \mathcal{H}|_{\phi=\nu=0} + \frac{C_\phi^2}{2M_*^2K_Bq^2} + \frac{3C_\nu^2}{4M_*^2}. \tag{70}$$

The equations propagated numerically are

$$\dot{x} = \partial_P\mathcal{H}_{\mathrm{red}}, \qquad \dot{P} = -\partial_x\mathcal{H}_{\mathrm{red}} - 3HP. \tag{71}$$

A changing sign in the momentum quadratic form does not make these constraint equations singular. It does change the interpretation of the reduced dynamics and must be retained in its diagnosis.

7 An exact momentum-positivity criterion

Let $\mathsf{R} = \partial_P\partial_P\mathcal{H}_{\mathrm{red}}$. Equations (65)–(68) give

$$\mathsf{R} = G_4^{-1} + \frac{ww^T}{M_*^2K_Bq^2} + \frac{3\ell\ell^T}{2M_*^2}, \qquad w = (H, Q, v, 0)^T, \quad \ell = (1/3, 0, 0, 1)^T. \tag{72}$$

Define

$$\mathcal{D} = (2M_*^2 H - \gamma v)^2 - M_*^2 K_B \rho_d, \tag{73}$$

$$\mathcal{T} = -6M_*^2 H^2 + 2M_*^2 K_2 Q^2 + v^2 + 6\gamma H v, \tag{74}$$

$$\mathcal{N} = \mathcal{D} q^2 - \rho_d \mathcal{T}. \tag{75}$$

Proposition 2. *For $M_*^2, K_2, K_B, \rho_d, q^2 > 0$, the matrix R is positive definite if and only if $\mathcal{N} > 0$. It has exactly one negative direction for $\mathcal{N} < 0$, and exactly one zero direction for $\mathcal{N} = 0$.*

Proof. The principal (χ, s, δ_N) block of G_4^{-1} is

$$\operatorname{diag}\left(\frac{1}{2M_*^2 K_2}, \frac{2M_*^2}{2M_*^2 + 3\gamma^2}, \frac{q^2}{\rho_d}\right) > 0. \tag{76}$$

The two rank-one additions in (72) are positive semidefinite. The corresponding three-dimensional principal block of R is therefore strictly positive. Its Schur complement is a scalar and determines the remaining sign. Direct evaluation gives

$$\det \mathsf{R} = \frac{\mathcal{N}}{4K_2 K_B (M_*^2)^3 q^2 \rho_d (2M_*^2 + 3\gamma^2)}. \tag{77}$$

The denominator is positive, which proves all three statements. □

The full Friedmann equation makes the coefficient $\mathcal{T}$ much simpler. Since $\rho_Q = M_*^2 K_2 (Q^2 - Q_0^2)$, substitution of (13) and (15) into (74) gives

$$\boxed{\mathcal{T} = 2M_*^2 K_2 Q_0^2 - 2\rho_d - m_\Sigma^2 \Sigma^2.} \tag{78}$$

All explicit field velocities cancel. The derivative coupling still affects $\mathcal{D}$ and the background trajectory, so this simplification does not remove memory dynamics from the criterion.

The dimensions are $[\mathcal{D}] = 6$, $[\mathcal{T}] = 4$, and $[\mathcal{N}] = 8$. If $\mathcal{D} > 0$ and $\mathcal{T} > 0$, positivity requires

$$q^2 > q_{\rm kin}^2, \qquad q_{\rm kin}^2 = \frac{\rho_d \mathcal{T}}{\mathcal{D}}. \tag{79}$$

Other sign combinations must be handled with (75), rather than assuming a positive threshold. In particular $\mathcal{D} > 0$, $\mathcal{T} \le 0$ gives positivity for every nonzero q, whereas $\mathcal{D} < 0$, $\mathcal{T} \ge 0$ gives none. When both are negative, a low-q positive interval can exist. The cases $q = 0$ and $\rho_d = 0$ require a different set of reduced variables; the inverses used in the proof are then unavailable.

7.1 A late-time restriction

Corollary 1. *Suppose a solution expands to $a \to \infty$, with $Q_0 \neq 0$, $\rho_d = \rho_{d0} a^{-3}(1 + o(1))$, $\rho_{d0} > 0$, and $H, \Sigma, v = O(a^{-3/2})$. In the zero-cosmological-constant model specified above, every fixed finite $k > 0$ eventually has $\mathcal{N} < 0$.*

Proof. The stated falloffs give $\mathcal{D} = O(a^{-3})$ and $\mathcal{T} = 2M_*^2 K_2 Q_0^2 + o(1) > 0$. Since $q^2 = k^2/a^2$,

$$\mathcal{N} = O(a^{-5}) - 2\rho_{d0} M_*^2 K_2 Q_0^2 a^{-3}(1 + o(1)), \tag{80}$$

whose leading coefficient is negative. □

Thus an indefinitely positive momentum form for every fixed comoving scalar mode cannot be imposed on this asymptotically dust-like branch. The conclusion does not assume that such a branch attracts all solutions. A nonzero cosmological constant, a nondecaying memory or $Q_0 = 0$ changes the premises. Appendix D exhibits another homogeneous branch, but finds it to be a saddle rather than a demonstrated late-time attractor.

A conditional scale from recombination. The asymptotic restriction can become relevant well before the far future if the scalar remnant is identified with cold dark matter. To make that statement precise, suppose production has ended before recombination, $Q_0 C_Q > 0$, the domain density is identified with baryons, and $\rho_c = M_*^2 Q_0 C_Q / a^3$ supplies the cold component. Define the stiff-to-dust energy ratio

$$q_s(a) \equiv \frac{\rho_{Q,\mathrm{stiff}}}{\rho_c} = \frac{C_Q}{4K_2 Q_0 a^3}, \qquad 2M_*^2 K_2 Q_0^2 = \frac{\rho_c}{2q_s}. \tag{81}$$

Here q_s is dimensionless and is distinct from the physical wavenumber q. For constant C_Q, an illustrative requirement $q_s(a_{\mathrm{rec}}) \lesssim 10^{-2}$ at $z_{\mathrm{rec}} \simeq 1100$ gives

$$q_{s0} \lesssim \frac{10^{-2}}{1101^3} = 7.49 \times 10^{-12}. \tag{82}$$

The one-percent choice is a stiff-energy benchmark, not a bound inferred from Planck and not a sufficient condition for cold-dark-matter clustering. If charge production continues after recombination, $q_{s0} = q_s(a_{\mathrm{rec}})(C_{Q_0}/C_{Q_{\mathrm{rec}}})a_{\mathrm{rec}}^3$, and (82) does not follow without controlling that ratio.

Assume also $|\gamma v| \ll M_*^2 H$ and $2\rho_d + m_\Sigma^2 \Sigma^2 \ll \rho_c/(2q_s)$. With $\Omega_b = \rho_d/(3M_*^2H^2)$ and $\Omega_c = \rho_c/(3M_*^2H^2)$, (79) becomes

$$\boxed{q_{\mathrm{kin}}^2 \simeq \frac{9\Omega_b\Omega_c}{2(4 - 3K_B\Omega_b)}\frac{H^2}{q_s} \simeq \frac{9}{8}\Omega_b\Omega_c\frac{H^2}{q_s}.} \tag{83}$$

The second expression additionally drops $3K_B\Omega_b$ relative to 4. The explicit K_2 dependence cancels at fixed remnant density and stiff fraction. This does not remove the dependence of their production history on K_2. If the derivative mixing is appreciable, the denominator in the first expression instead contains $4(1-\eta)^2 - 3K_B\Omega_b$, where $\eta = \gamma v/(2M_*^2 H)$; the simple numerical estimate then need not apply.

For a conditional present-day normalization, use $h = 0.674$, $\Omega_{b0}h^2 = 0.02237$ and $\Omega_{c0}h^2 = 0.1200$ from the base-ΛCDM Planck analysis [20], identifying its critical-density coefficient with M_*^2. Dropping the K_B correction gives $q_{\mathrm{kin},0} \gtrsim 4.42 \times 10^4 H_0$. Restoring c for the conversion and defining the wavelength as $\lambda_{\mathrm{kin}} = 2\pi/q_{\mathrm{kin}}$, rather than $1/q_{\mathrm{kin}}$, gives

$$\lambda_{\mathrm{kin},0} \lesssim 0.632 \text{ Mpc}. \tag{84}$$

Keeping $K_B = 1$ gives $q_{\mathrm{kin},0}/H_0 \gtrsim 4.50 \times 10^4$ and $\lambda_{\mathrm{kin},0} \lesssim 0.621$ Mpc. Under these matching assumptions, wavelengths above approximately 0.63 Mpc, including the usual large-scale linear-structure wavelengths, already have a nonpositive momentum form. The quoted length is an upper bound at the chosen coldness threshold, not a universally selected scale.

There is an essential background qualification. The observed present-day values $\Omega_{b0} + \Omega_{c0} \simeq 0.313$ are not a solution of our flat, zero-Λ, negligible-memory dust background, which requires a total matter fraction near unity. Equation (84) is therefore a late-background matching estimate, not an on-shell prediction of that restricted model. For example, adding a constant density ρ_Λ leaves the momentum matrix (72) unchanged but replaces (78) by $\mathcal{T} = \rho_c/(2q_s) - 2\rho_d - m_\Sigma^2\Sigma^2 - 2\rho_\Lambda$. When the first term dominates, (83) remains the leading estimate. Such an added component is not present in the simulations or in Corollary 1.

During strict matter domination, Ω_b and Ω_c are constant, and H^2 and q_s both scale as a^{-3}. Hence the physical boundary is approximately constant. Using the same physical baryon and cold densities to extrapolate a matter-only background, $H_{\mathrm{m}}^2 = H_0^2(\Omega_{b0} + \Omega_{c0})a^{-3}$, gives $\lambda_{\mathrm{kin}} \lesssim 0.354$ Mpc in the second approximation of (83), or 0.333 Mpc for $K_B = 1$. At saturation these are of the order of the physical recombination Hubble length, but no equality with a particle or sound

horizon is implied; radiation also matters near recombination. A late accelerating background changes the constant-matter-era scaling and accounts for the different present-day estimate. This conditional calculation makes the physical canonical interpretation of the infrared mode urgent for any cold-dark-matter identification; it does not by itself establish a fatal quantum instability.

Comparison with a Jeans estimate. After production, the adiabatic ratio of the isolated homogeneous charge sector is $c_a^2 = \dot{p}_Q/\dot{\rho}_Q = 2q_s/(1+2q_s)$. If one defines only for comparison a physical Newtonian wavenumber $q_{J,\mathrm{ad}}^2 = 4\pi G\rho_c/c_a^2$, with $8\pi G = 1/M_*^2$, Eq. (83) gives

$$\frac{q_{\mathrm{kin}}^2}{q_{J,\mathrm{ad}}^2} \simeq \frac{6\Omega_b}{(4-3K_B\Omega_b)(1+2q_s)}. \tag{85}$$

This formal ratio is not an identification of the physical coupled mode. Even in the memory-decoupled, matter-free Minkowski limit, eliminating the lapse gives the propagating scalar coefficient

$$c_{\mathrm{sc}}^2 = \frac{A(2+K_Bj)}{2K_2K_B}, \qquad \omega^2 = c_{\mathrm{sc}}^2q^2 + \frac{A(1+j)}{K_B}Q_0^2, \tag{86}$$

in agreement with the corresponding AeST limit [12]. The bare gradient/velocity ratio $A(1+j)/(2K_2)$ is not this speed. For the expanding coupled system, its physical modes, effective gravitational response and transfer functions remain to be calculated. Satellite counts [22] and Lyman-α data [23] constrain specified suppression histories; their thermal-relic free-streaming limits cannot be assigned directly to $2\pi/q_{\mathrm{kin}}$.

7.2 What this criterion does and does not establish

Proposition 2 is a necessary and sufficient statement about the momentum block in the specified representation, not about the complete Hamiltonian, the entire spectrum, or quantum stability. A positive momentum block can coexist with attractive growing modes, as the calculations below show. Conversely, an infrared negative kinetic or momentum term can require a canonical and dynamical interpretation rather than an immediate ultraviolet-ghost conclusion. This issue is explicit in the AeST stability analysis [12]; examples in other theories show how an infrared ghost-like description can represent a Jeans instability [24]. Those examples do not establish that the present extension is safe.

A physical classification would additionally require the relevant mode variables, their evolution and interaction scale, and the cutoff of this effective action. We therefore call (79) a momentum-positivity boundary, not a measured Jeans scale or a universal exclusion bound. The useful exact result is that the apparently complicated four-field sign question has a single algebraic answer, and that its dust-like asymptotic limitation is unavoidable under the stated assumptions.

Figure 2 illustrates the boundary on the reference background used below.

8 Initial conditions, entropy and full transfer matrices

8.1 Separating a response basis from primordial statistics

Under a first-order time displacement T, $\delta_n \mapsto \delta_n + 3HT$ and $\delta X \mapsto \delta X - \dot{X}T$ for a background scalar X. For $H \neq 0$, the combinations

$$\mathcal{S}_{\Sigma n} = s + \frac{v}{3H}\delta_n, \quad \mathcal{S}_{\vartheta n} = \chi + \frac{Q}{3H}\delta_n, \quad \mathcal{S}_{\kappa n} = \delta\kappa + \frac{\dot{\kappa}}{3H}\delta_n \tag{87}$$

are gauge invariant. A common local-clock displacement makes them vanish. These conditions identify relative scalar fluctuations in the standard spirit of cosmological entropy perturbations [25]; they do not fix relative velocities or a complete primordial mode at finite k.

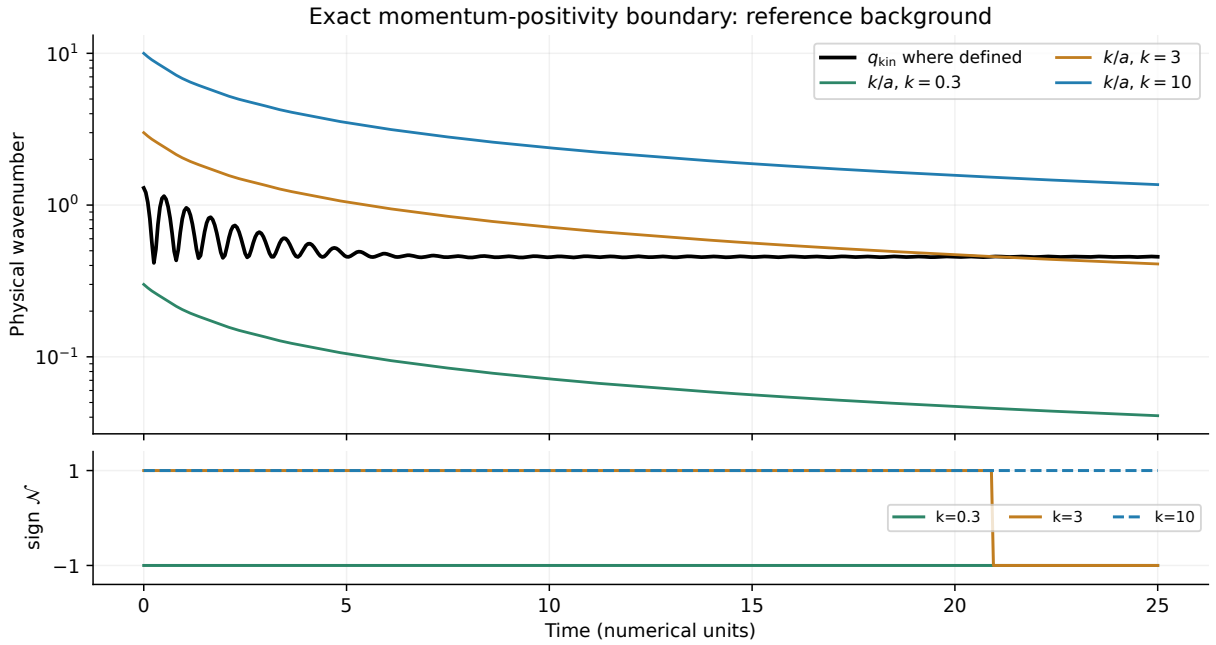


Figure 2: Momentum-positivity boundary for the reference background. The upper panel compares physical wavenumbers k/a with $q_{\rm kin}$ only where $\mathcal{D}, \mathcal{T} > 0$. The lower panel gives the sign of $\mathcal{N}$, evaluated directly rather than extending an inapplicable threshold formula. A positive sign is not a full stability criterion. All scales are in the numerical normalization.

The number contrast in Newtonian gauge is obtained from

$$\Psi_{\rm N} = -\zeta - HB = -\zeta + \frac{H\nu}{q^2}, \qquad \delta_{n,\rm N} = \delta_N + 3\Psi_{\rm N}. \tag{88}$$

The local charge perturbation in aether-normal gauge is

$$\delta\kappa = \frac{2M_*^2 K_2(\dot\chi - Q\phi) - \bar q\delta_n}{n}, \qquad \bar q = M_*^2\mathcal{K}_Q. \tag{89}$$

It transforms to Newtonian gauge as $\delta\kappa_{\rm N} = \delta\kappa + \dot\kappa B$. We specify the gauge whenever using $\delta\kappa$ before the source has ended.

Let $Y = (x, P)^T$ and H be the Hessian of $\mathcal{H}_{\rm red}$. Then

$$\dot Y = \mathsf{L}(t,k)Y, \qquad \mathsf{L} = \begin{pmatrix} \mathsf{H}_{Px} & \mathsf{H}_{PP} \\ -\mathsf{H}_{xx} & -\mathsf{H}_{xP} - 3H\mathbf{1}_4 \end{pmatrix}. \tag{90}$$

We propagate the full fundamental matrix Z, with $\dot Z = \mathsf{L}Z$ and $Z(t_i) = \mathbf{1}_8$. Any constraint-compatible initial response then follows from $Y(t) = Z(t)Y_i$. For $a_i = 1$,

$$Z^T J Z = a^{-3}J, \qquad J = \begin{pmatrix} 0 & \mathbf{1}_4 \\ -\mathbf{1}_4 & 0 \end{pmatrix}, \tag{91}$$

because P is normalized by a^3. Singular values of Z in raw numerical coordinates depend on field units and are not physical amplification observables. A predicted power spectrum would require an independently justified initial covariance; none is assumed here.

8.2 Benchmarks and independent checks

The calculations use dimensionless numerical values

$$\begin{gathered} M_*^2 = 1, \quad K_2 = 10, \quad Q_0 = 0.5, \quad m_\Sigma = 5, \quad f = 1, \\ n_0 = 0.2, \quad M_d = 0.2, \quad p = 4, \quad \gamma = 0.1, \quad K_B = j = 1. \end{gathered} \tag{92}$$

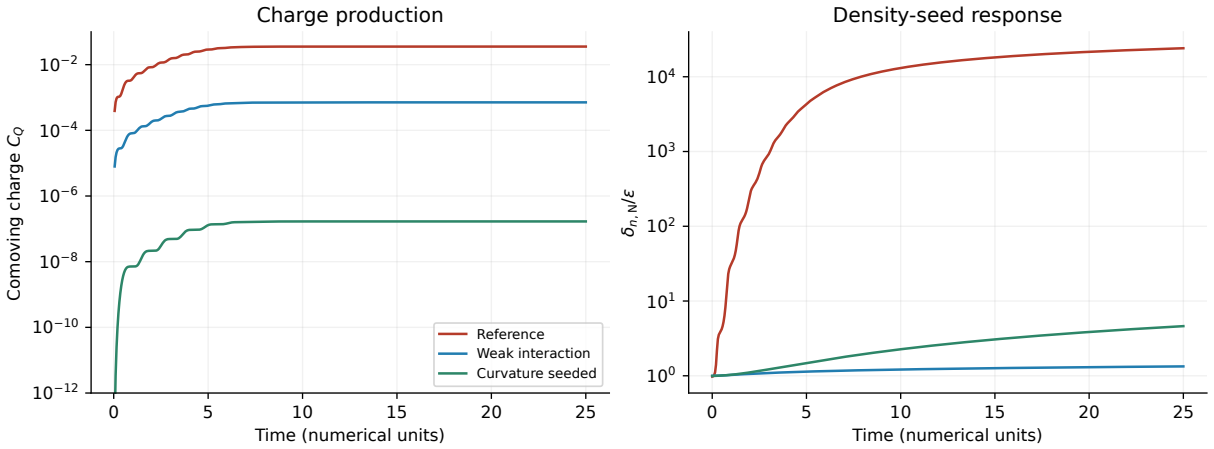


Figure 3: Homogeneous charge and Newtonian density response from the density-seed transfer column, in the dimensionless benchmarks of Table 1. The density response is divided by the initial coordinate-number amplitude ϵ; a symmetric logarithmic scale preserves sign and the vicinity of zero. Homogeneous production and spatial amplification are visibly different outputs.

We set $a_i = 1$, $\vartheta_i = C_{Q_i} = v_i = 0$, $F_i = 0.99$, with H_i fixed by Friedmann. The reference has $E = 50$, $\Sigma_i = 0.2$; the weak-interaction case has $E = 1$; the curvature-seeded case has $E = 50$, $\Sigma_i = 0$. These are synthetic effective-equation benchmarks. They are not parameter values fitted to cosmological time, a measured Planck scale or an observational wavelength. An effective cutoff has not been supplied. In particular, the numerical ratio $m_\Sigma/M_* = 5$ is not asserted to lie within a controlled gravitational effective regime; these runs demonstrate the equations and their response, not a physically calibrated parameter window.

For the new density response, choose

$$x_i = \epsilon(0, 0, 0, 1)^T, \qquad \dot{\zeta}_i = \dot{s}_i = \dot{\delta}_{N,i} = 0, \qquad \delta Q_i = 0. \tag{93}$$

The lapse, shift and $\dot{\chi}_i = Q_i\phi_i$ are solved jointly. They cannot all be independently set to zero. This is a well-defined response column, not a primordial adiabatic mode: for example $\mathcal{S}_{\vartheta n,i} = Q_i\epsilon/(3H_i) \neq 0$. A second initial condition, used for comparison, has $x_i = \epsilon(0, 0, \Sigma_i, 0)^T$ with the same velocity and proper-Q conditions.

The background and modes are integrated with DOP853, maximum step 0.04, and relative and absolute mode tolerances 2×10^{-10} and 2×10^{-12}. A two-order tolerance tightening changes the reference memory-seed final Newtonian density response by 5.3×10^{-11} in relative terms. Applying the independently propagated Z to three earlier directly integrated memory-seed states reproduces their final phase-space vectors with maximum normalized discrepancy 5.2×10^{-11}.

Further checks do not rely solely on integrating the same equations twice. A direct expansion of the unexpanded ADM and material-label action at twelve background/wavenumber samples agrees with the quadratic action to 1.5×10^{-8} in normalized residual. The Hamiltonian constraint block is checked symbolically and numerically. The sampled Friedmann residual in the seven direct mode runs is below 1.6×10^{-10}. An independently integrated current balance, given in Appendix B, agrees with (89) below 1.3×10^{-11} in normalized residual. The sign criterion agrees with numerical inertia at all 2,004 sampled states of the four matrix runs.

Equation (91) is also checked, with maximum residual below 1.7×10^{-11} after division by $1 + \|Z\|_F^2$. This is a scale-normalized consistency diagnostic; it does not guarantee accuracy of every small singular value of an ill-conditioned transfer matrix. The recorded results and source code retain the normalization and all cases.

Case	k	$C_Q(t_f)$	$\delta_{n,\mathrm{N}}/\epsilon$	$\delta\kappa/\epsilon$	n_-
Reference	10	$3.55746\,10^{-2}$	24063.0	−4160.19	0
Weak interaction	10	$7.11204\,10^{-4}$	1.33492	0.0302256	0
Curvature seeded	10	$1.68188\,10^{-7}$	4.61338	0.447022	0, 1
Reference, infrared	0.3	$3.55746\,10^{-2}$	1.82855	−0.231238	1

Table 1: Full transfer-matrix response to (93) at $t_f = 25$. The charge perturbation uses aether-normal gauge. n_- lists the numbers of negative momentum directions encountered, not a stability verdict. Values are response coefficients per coordinate-number seed ϵ, not growth factors normalized to an initial Newtonian contrast. The weak-interaction row demonstrates a modest response for this initial condition and interval only.

8.3 Production, redistribution and initial-condition sensitivity

Table 1 and Fig. 3 give the density-seed responses. The reference produces a regular positive homogeneous charge while generating a large density response, even though its momentum block remains positive at $k = 10$ over the integration interval. Reducing E gives a much smaller charge and a modest density response for the same initial column. At $k = 0.3$, the reference has one negative momentum direction throughout the sampled interval, but a much smaller density response. Neither the sign criterion nor the final homogeneous charge alone orders the amount of amplification.

The curvature-seeded case produces a nonzero mean charge and a nonzero spatial response from $\Sigma_i = v_i = C_{Q_i} = s_i = 0$. This realizes the mechanism of (20) at the homogeneous and linear-response levels. Its mean charge is very small and it crosses into a region with one negative momentum direction. A fractional charge perturbation divided by that tiny mean can be large without a comparably large absolute charge density; it must not be used as evidence of successful structure formation.

The initial-condition dependence is substantial. For the reference at $k = 10$, the memory-seed column gives $\delta_{n,\mathrm{N}}/\epsilon = -84080.8$, whereas the density-seed column gives 24063.0. The corresponding weak-interaction responses are −12.1898 and 1.33492. These are linear response coefficients, so ϵ must be small enough that all perturbations remain within the linear regime. They do not assign a probability to either initial condition.

The current balance gives a sharper diagnosis of retention. In the reference memory-seed run,

$$\frac{\delta\kappa(t_f)}{\epsilon} = 14546.67 = 100.41 + 14446.26, \tag{94}$$

where the last two terms are respectively the integrated local source and relative-flux contributions in the declared gauge. At t_f, $F \simeq 1.37 \times 10^{-9}$. The spatial flux, not the local production perturbation, dominates this particular final charge-per-domain response. Figure 4 displays this separation; it is the direct numerical counterpart of (56). It cannot be inferred from the homogeneous charge curve.

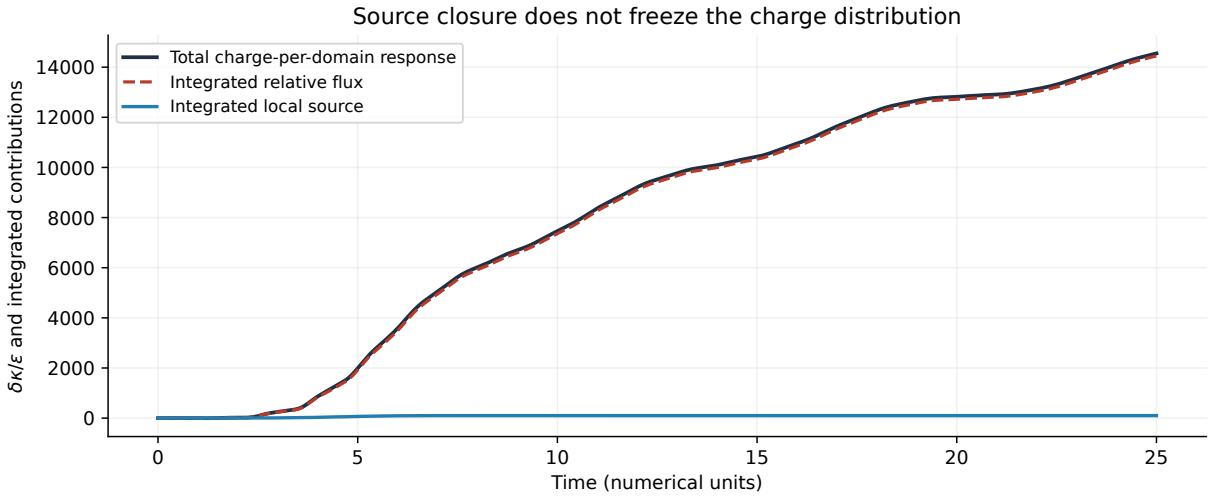


Figure 4: Reference memory-seed response at $k = 10$: total charge-per-domain perturbation and the time integrals of its local-source and relative-flux terms. The balance is checked against the independently reconstructed charge. Quantities use aether-normal gauge and are divided by the initial memory-seed parameter ϵ. The source window closes while spatial redistribution continues.

9 Implications and limits

The results connect the geometry, its material response and a conditional quantum channel. The geometric switch specifies a rest-energy interaction and therefore a homogeneous charge source, force and relative current. Positivity of the produced dust-like term fixes the sign of the opening clock. With a common aperture, this clock also controls the remaining resolving action. The finite-budget theorem makes sustained localization a new condition on the state dependence of the microscopic noise, alongside the independent requirements of retention and cold clustering.

This structure also identifies three independent obstructions to a simple interpretation. First, the force can remain active outside the narrow production window. Second, charge can move relative to its original carriers after production stops. Third, on the stated dust-like asymptotic branch, maintaining a positive momentum form for a fixed comoving mode indefinitely is impossible. The first two are statements about action-derived physical exchange. The third is a precise representation-dependent restriction that calls for a further infrared dynamical classification.

None of these results requires identifying decoherence with charge. The localization and reconstruction preprints [3, 4] motivate treating the aperture state and its response kernel seriously, but a completely positive quantum generator, by itself, does not provide the energy budget or current in (5). A microscopic completion would have to derive the interaction, its fluctuations and its energy exchange rather than borrow a localization rate as a charge-production law.

The susceptibility construction adds no present cosmological observable. Its directly testable content is the laboratory Hill-curvature relation and the normalization-free null identity derived in Section 4.2. For a positive domain population, the same switch also implies one-sided consistency bounds on the reduced production profile. These bounds are not constraints on an arbitrary physical source history: they require an independently reconstructed reduced profile and a specified parameter point that fixes the memory history and opening clock. If the population-induced memory loading is non-negligible, the population weight and Σ must be inferred jointly. The positive-population inequalities should therefore be regarded as exclusion conditions of principle until a cosmological observable reconstructs the relevant production history.

The remaining limitations are concrete. There is no physical calibration of the numerical parameters, no radiation-era or primordial-state construction, no calculated initial covariance, and no effective cutoff or strong-coupling bound. Scalar evolution is treated linearly around a cold single-stream material continuum; domain formation and nonlinear multistreaming are absent. Vector and tensor perturbations during transfer have not been analysed here. We have not computed halos, lensing, the cosmic microwave background, or an abundance matching the dark sector. The absence of those results prevents a claim of cosmological viability, but does not weaken the conditional identities or propositions proved above.

Two linked developments now decide the common-origin interpretation. The classical sector requires a physical canonical interpretation of the infrared mode, its interaction scale and a primordial-state calculation. The quantum connection requires a local matching solution and a microscopic normalization/noise law with an energy budget. A bounded normalization and a homogeneous aperture following Eq. (22) cannot provide arbitrarily large remaining localization for a fixed domain. A compensating normalization, changing aperture density, local state separation or a different channel must be derived with its own backreaction. The conditional recombination estimate places this question on large-scale-structure wavelengths already at finite epochs if the remnant is assigned the cold-dark-matter abundance. The classical scalar evolution is specified, while the microscopic noise law and local matching remain to be supplied. Any modification intended to improve the response must be rechecked against the current, force and constraint relations together.

10 Conclusion

A covariant dynamical memory can generate a geometric scalar charge while fixing the associated material force and relative current. The charge can redistribute after local production ends. Its constrained scalar momentum form admits an exact algebraic positivity criterion, and every fixed nonzero comoving mode eventually leaves the positive region on the stated dust-like branch. The resulting infrared question is retained rather than interpreted away.

Combining this charge-producing representative with a common-aperture quantum channel yields a further restriction. A positive produced dust-like term requires an increasing homogeneous aperture at fixed proper aperture density. With bounded localization normalization, the integrated future resolving action is finite. Some attenuation targets then remain unreachable regardless of the waiting time. Its retrospective counterpart connects the accumulated aperture evolution to the thermal and ionization history of diffuse gas once a normalization history is specified or a positive lower bound on the past normalization is independently justified. The operational mass threshold moves with the aperture; for the declared reference regime its mass scales as $r_d^{18/7}$. A state-dependent rate can evade the finite budget, but infinite event activity alone does not suffice: the activation and resolving thresholds differ by two powers of the aperture.

A laboratory size scan can additionally test the declared Hill switching law through a normalization-free slope–curvature identity. If the same switch is retained in the memory sector, positivity of a conserved domain population places one-sided bounds on the width and low-frequency Fourier content of the reduced charge-production profile. These are consistency conditions of principle rather than present cosmological tests: their empirical use requires an independently reconstructed production history and a specified dynamical parameter point fixing the memory field and the absolute opening clock.

These results identify a concrete task for a microscopic common origin. It must jointly account for charge generation, spatial dynamics, the evolution of localization strength and the energy supplied by its fluctuations. The finite-budget result is a conditional theorem for the specified channel and clock, not a prediction that previously classical objects recover coherence, and not a complete quantum-cosmological solution. Its force is that the geometrical remnant

and sustained intrinsic localization can no longer be treated as independent outputs of that realization.

Declarations

Funding. This research received no external funding.

Competing interests. The author declares no competing interests. The affiliation with Precog Technologies is provided as a professional affiliation; Precog Technologies did not fund, sponsor or commission the work reported in this manuscript.

Data availability. No new observational or experimental data set was generated or reanalysed in this study. Numerical verification code, machine-readable outputs and figure-generation scripts supporting the reported calculations are supplied as supplementary material with the manuscript. These include `verify_theorems.py`, `check_formulas.py`, `verify_modes.py`, `check_recombination.py`, `check_localization_budget.py`, `check_susceptibility_bounds.py`, the scalar solver in `calculations/`, and the corresponding JSON and NPZ results. Published cosmological benchmarks are taken from the cited literature.

A Complete quadratic scalar action

All coefficients below are evaluated on the background solution. Put $d = (\dot\zeta, \dot\chi, \dot s)^T$, $w_3 = (H, Q, v)^T$, and let G_3 be the upper 3×3 block of (65). Up to boundary terms, the quadratic action per Fourier mode is $\int \mathrm{d}t\, a^3\mathcal{L}_2$, with

$$\mathcal{L}_2 = \mathcal{L}_{\rm hom} + \mathcal{L}_{\rm grad} + \mathcal{L}_{\rm shift} + \mathcal{L}_{\rm dom}. \tag{95}$$

For real Fourier amplitudes with a common normalization,

$$\begin{aligned}
\mathcal{L}_{\rm hom} &= \tfrac{1}{2}(d-\phi w_3)^T G_3 (d-\phi w_3) - \tfrac{1}{2}m_\Sigma^2 s^2 - m_\Sigma^2\Sigma\phi s \\
&\quad + 3\zeta\big[\Pi\cdot d + (f_0 - \Pi\cdot w_3)\phi - m_\Sigma^2\Sigma s\big] + \tfrac{9}{2}f_0\zeta^2, && (96)\\
\mathcal{L}_{\rm grad} &= M_*^2 q^2(\zeta^2 + 2\phi\zeta) + \tfrac{1}{2}M_*^2 K_B q^2\phi^2 + M_*^2 A q^2\phi\chi \\
&\quad - \tfrac{1}{2}M_*^2 A(1+j)q^2\chi^2 - \tfrac{1}{2}q^2 s^2 - \gamma q^2\phi s, && (97)\\
\mathcal{L}_{\rm shift} &= \nu\big[2M_*^2\dot\zeta - \gamma\dot s - (2M_*^2 H - \gamma v)\phi + \Pi_\vartheta\chi + \Pi_\Sigma s\big], && (98)\\
\mathcal{L}_{\rm dom} &= \frac{\rho_d}{2q^2}(\dot\delta_N - \nu)^2 - \frac{n}{2}\big[U_{\vartheta\vartheta}\chi^2 + 2U_{\vartheta\Sigma}\chi s + U_{\Sigma\Sigma}s^2\big] \\
&\quad - n\phi(U_\vartheta\chi + U_\Sigma s) - n\delta_N(\mu\phi + U_\vartheta\chi + U_\Sigma s). && (99)
\end{aligned}$$

The label formulation explains why the rest-energy term has no independent $\zeta\delta_N$ contribution: the conserved coordinate number multiplies $N\mu$, while proper density supplies the inverse volume factor. The kinetic term follows from the domain velocity relative to the shift. The memory mixing in ADM form is $\gamma V_\Sigma K - \gamma D_i\Sigma D^i \ln N$, where $V_\Sigma = u^\mu\nabla_\mu\Sigma$ and K is the trace of the extrinsic curvature. These expressions permit a direct expansion independent of the reduced Hamiltonian.

For implementation, write

$$\mathcal{L}_2 = \tfrac{1}{2}\dot x^T G\dot x + \dot x^T B x + \dot x^T D c + \tfrac{1}{2}x^T C x + x^T E c + \tfrac{1}{2}c^T A_c c. \tag{100}$$

Then $P = G\dot x + Bx + Dc$. Legendre transforming with this relation, rather than eliminating c in a possibly singular velocity representation, gives (66). The supplied code constructs these matrices from (96)–(99), takes the Schur complement of the Hamiltonian constraint block, and evolves (71).

B An independent perturbative current balance

Linearizing (56) in aether-normal gauge gives

$$\delta\dot{\kappa} = -U_{\vartheta\vartheta}\chi - U_{\vartheta\Sigma}s - \phi U_{\vartheta} - \frac{\mathcal{D}_{\rm flux}}{n}, \tag{101}$$

$$\mathcal{D}_{\rm flux} = M_*^2 A q^2[(1+j)\chi - \phi] + \bar{q}(\dot{\delta}_N - \nu). \tag{102}$$

The first part of (102) is the intrinsic current relative to the aether; the second accounts for the material velocity relative to that frame. The lapse term in (101) is essential because background production is measured in proper time. Integrating this equation independently and comparing with (89) tests the source, shift and force conventions simultaneously. The local-source/flux split is gauge dependent while production is active, and all numerical values of that split in this paper use the explicitly stated gauge. Once $\dot{\kappa} = 0$, $\delta\kappa$ itself is invariant under linear time shifts.

C Positive-population deconvolution criterion

For the normalized convolution in Section 4, the formal deconvolution is

$$\widehat{w}(k) = \frac{\widehat{j}(k)}{\widehat{P}_p(k)}, \qquad \widehat{P}_p(k) = \frac{\pi k/p}{\sinh(\pi k/p)}, \tag{103}$$

because $\widehat{P}_p(k) \neq 0$ for real k. A normalized deconvolution corresponds to a positive population if and only if $\widehat{w}$ is a characteristic function. By Bochner's theorem this is equivalent to positive definiteness: for every finite set $\{k_i\}_{i=1}^N$,

$$\left[\frac{\widehat{j}(k_i - k_j)}{\widehat{P}_p(k_i - k_j)}\right]_{i,j=1}^{N} \succeq 0. \tag{104}$$

This criterion is mathematically complete but statistically ill conditioned at large $|k|$, because $\widehat{P}_p(k)$ decreases exponentially. The variance bound and the low-frequency envelope in the main text are therefore the preferred practical diagnostics.

D A memory-supported de Sitter saddle

The dust-like asymptotic assumptions in Corollary 1 are not automatic. In the homogeneous sector with $n = C_Q = 0$, $Q = Q_0$, $v = 0$ and constant $H > 0$, the field equations require

$$3M_*^2H^2 = \tfrac{1}{2}m_\Sigma^2\Sigma^2, \qquad m_\Sigma^2\Sigma + 9\gamma H^2 = 0. \tag{105}$$

Besides the zero-curvature solution, for $\gamma \neq 0$ and $m_\Sigma > 0$ there is

$$\Sigma_{\rm dS} = -\frac{2M_*^2}{3\gamma}, \qquad H_{\rm dS}^2 = \frac{2M_*^2 m_\Sigma^2}{27\gamma^2}. \tag{106}$$

It is not a stable homogeneous attractor. On the fixed-zero-charge, zero-domain subspace, the linearized Friedmann constraint gives

$$\delta H = -\frac{3\gamma H_{\rm dS}}{2M_*^2}\delta\Sigma + \frac{\gamma}{2M_*^2}\delta\dot{\Sigma}. \tag{107}$$

Substitution into (18) yields

$$\delta\ddot{\Sigma} + 3H_{\rm dS}\delta\dot{\Sigma} - \frac{2M_*^2 m_\Sigma^2}{2M_*^2 + 3\gamma^2}\delta\Sigma = 0. \tag{108}$$

The exponents are

$$\lambda_{\pm} = \frac{-3H_{\rm dS} \pm \sqrt{9H_{\rm dS}^2 + 8M_*^2 m_\Sigma^2/(2M_*^2 + 3\gamma^2)}}{2}, \tag{109}$$

with one positive and one negative value. An unstable direction in this invariant subspace is already sufficient to rule out homogeneous attraction in the full system. This branch therefore cannot be invoked as a demonstrated dark-energy completion. Its $\gamma \to 0$ limit also moves to unbounded field and curvature, where the effective action may be inapplicable. The four-coordinate dust reduction of Section 6, which assumes $\rho_d > 0$, is not used in this calculation.

E Reproducibility and scope of the results

The accompanying source archive includes the symbolic checks, background and scalar solvers, recorded JSON and NPZ results, and scripts generating all four figures. `verify_theorems.py` checks the Friedmann cancellation, principal block and de Sitter linearization; the scalar solver `verify_flrw.py` in `calculations/` checks the constraint determinant and independent action expansion and reproduces the direct perturbation runs; `verify_modes.py` reproduces the four fundamental matrices. `crosscheck_transfer.py` compares these with the direct evolutions. No observational dataset is reanalysed. Published cosmological parameter values are used only for the conditional recombination estimate; `check_recombination.py` and `recombination_results.json` reproduce its algebra and numerical conversions.

The additional script `check_localization_budget.py` verifies the exact opening-dependent rate and threshold derivatives, the event integral, and an analytic dust–stiff background against an independent ODE solution. It also computes the finite-budget examples and their normalization-exponent alternatives, with quadrature tail bounds. Its JSON and NPZ outputs and the localization figure are supplied. The static-aperture and rapidly increasing-normalization counterexamples are retained.

The script `check_susceptibility_bounds.py` independently checks the Hill slope–curvature identities, the logistic-kernel normalization and variance, the Fourier transform against numerical quadrature, the one-sided variance bound on positive mixtures, and the algebraic opening-clock corollary. Its machine-readable output is `susceptibility_bounds_results.json`.

The exact current identity follows directly from the proposed action. The force identity and positivity theorem are conditional deductions within it. The numerical responses are examples over a finite interval, not universal bounds. The late-time corollary is an asymptotic theorem under its stated falloffs, whereas the interaction and its geometric interpretation remain effective hypotheses. No external publication or independent review is implied by the reproducibility checks.

References

[1] Anisse Zerouta. Gravity as geometric filtration: A unified framework for cosmological and quantum phenomena. Research Square preprint, version 1. URL https://doi.org/10.21203/rs.3.rs-6570489/v1.

[2] Anisse Zerouta. DJAMILAR: Gravity as geometric filtration—a common geometric origin of gravitation, quantum-classical behaviour and dark-sector phenomenology. Research Square preprint, version 1. URL https://doi.org/10.21203/rs.3.rs-11144964/v1.

[3] Anisse Zerouta. Djamilar-induced localization and the quantum-classical transition. Research Square preprint, version 1. URL https://doi.org/10.21203/rs.3.rs-11162349/v1.

[4] Anisse Zerouta. DJAMILAR: Reconstructing the geometry of the quantum-classical transition—a common-aperture test linking matter-wave coherence and mechanical fluctuations. Research Square preprint, version 1. URL https://doi.org/10.21203/rs.3.rs-11189947/v1.

[5] Antoine Tilloy. Ghirardi–Rimini–Weber model with massive flashes. *Physical Review D*, 97:021502, 2018. doi: 10.1103/PhysRevD.97.021502. URL https://doi.org/10.1103/PhysRevD.97.021502.

[6] Nicolò Piccione. Diffusion minimization via optimal smearing in collapse and hybrid classical–quantum gravitational models. *Physical Review A*, 113:062211, 2026. doi: 10.1103/h74z-zvfv. URL https://doi.org/10.1103/h74z-zvfv.

[7] Thibault Damour, G. W. Gibbons, and Carsten Gundlach. Dark matter, time-varying G, and a dilaton field. *Physical Review Letters*, 64:123–126, 1990. doi: 10.1103/PhysRevLett.64.123.

[8] Greg W. Anderson and Sean M. Carroll. Dark matter with time-dependent mass. arXiv:astro-ph/9711288, 1997. URL https://arxiv.org/abs/astro-ph/9711288.

[9] Luca Amendola. Coupled quintessence. *Physical Review D*, 62:043511, 2000. doi: 10.1103/PhysRevD.62.043511. URL https://arxiv.org/abs/astro-ph/9908023.

[10] Glennys R. Farrar and P. J. E. Peebles. Interacting dark matter and dark energy. *The Astrophysical Journal*, 604:1–11, 2004. doi: 10.1086/381728. URL https://arxiv.org/abs/astro-ph/0307316.

[11] Constantinos Skordis and Tom Zlosnik. New relativistic theory for modified newtonian dynamics. *Physical Review Letters*, 127:161302, 2021. doi: 10.1103/PhysRevLett.127.161302. URL https://arxiv.org/abs/2007.00082.

[12] Constantinos Skordis and Tom Zlosnik. Aether scalar tensor theory: Linear stability on Minkowski space. *Physical Review D*, 106:104041, 2022. doi: 10.1103/PhysRevD.106.104041. URL https://arxiv.org/abs/2109.13287.

[13] Marianthi Bataki, Constantinos Skordis, and Tom Zlosnik. Aether scalar tensor theory: Hamiltonian formalism. *Physical Review D*, 110:044015, 2024. doi: 10.1103/PhysRevD.110.044015. URL https://arxiv.org/abs/2307.15126.

[14] Nima Arkani-Hamed, Hsin-Chia Cheng, Markus A. Luty, and Shinji Mukohyama. Ghost condensation and a consistent IR modification of gravity. *Journal of High Energy Physics*, 2004(05):074, 2004. doi: 10.1088/1126-6708/2004/05/074. URL https://arxiv.org/abs/hep-th/0312099.

[15] J. David Brown. Action functionals for relativistic perfect fluids. *Classical and Quantum Gravity*, 10: 1579–1606, 1993. doi: 10.1088/0264-9381/10/8/017. URL https://arxiv.org/abs/gr-qc/9304026.

[16] Guillermo Ballesteros and Brando Bellazzini. Effective perfect fluids in cosmology. *Journal of Cosmology and Astroparticle Physics*, 2013(04):001, 2013. doi: 10.1088/1475-7516/2013/04/001. URL https://arxiv.org/abs/1210.1561.

[17] Bassano Vacchini. Theory of decoherence due to scattering events and Lévy processes. *Physical Review Letters*, 95:230402, 2005. doi: 10.1103/PhysRevLett.95.230402. URL https://arxiv.org/abs/quant-ph/0510127.

[18] Angelo Bassi, Kinjalk Lochan, Seema Satin, Tejinder P. Singh, and Hendrik Ulbricht. Models of wave-function collapse, underlying theories, and experimental tests. *Reviews of Modern Physics*, 85: 471–527, 2013. doi: 10.1103/RevModPhys.85.471. URL https://arxiv.org/abs/1204.4325.

[19] Andrea Smirne and Angelo Bassi. Dissipative continuous spontaneous localization (CSL) model. *Scientific Reports*, 5:12518, 2015. doi: 10.1038/srep12518. URL https://arxiv.org/abs/1408.6446.

[20] Planck Collaboration. Planck 2018 results. VI. cosmological parameters. *Astronomy and Astrophysics*, 641:A6, 2020. doi: 10.1051/0004-6361/201833910. URL https://arxiv.org/abs/1807.06209.

[21] Rachel Bean, Eanna E. Flanagan, and Mark Trodden. Adiabatic instability in coupled dark energy–dark matter models. *Physical Review D*, 78:023009, 2008. doi: 10.1103/PhysRevD.78.023009. URL https://arxiv.org/abs/0709.1128.

[22] E. O. Nadler et al. Constraints on dark matter properties from observations of Milky Way satellite galaxies. *Physical Review Letters*, 126:091101, 2021. doi: 10.1103/PhysRevLett.126.091101. URL https://arxiv.org/abs/2008.00022.

[23] Vid Iršič et al. New constraints on the free-streaming of warm dark matter from intermediate and small scale Lyman-α forest data. *Physical Review D*, 96:023522, 2017. doi: 10.1103/PhysRevD.96.023522. URL https://arxiv.org/abs/1702.01764.

[24] A. Emir Gümrükçüoğlu, Shinji Mukohyama, and Thomas P. Sotiriou. Low energy ghosts and the Jeans' instability. *Physical Review D*, 94:064001, 2016. doi: 10.1103/PhysRevD.94.064001. URL https://arxiv.org/abs/1606.00618.

[25] Karim A. Malik and David Wands. Cosmological perturbations. *Physics Reports*, 475:1–51, 2009. doi: 10.1016/j.physrep.2009.03.001. URL https://arxiv.org/abs/0809.4944.